Supporting information for: Hydration repulsion difference between ordered and disordered membranes due to cancellation of membrane–membrane and water-mediated interactions

Bartosz Kowalik,[†] Alexander Schlaich,[†] Matej Kanduč,[‡] Emanuel Schneck,[¶] and Roland R. Netz[*,†]

†*Department of Physics, Freie Universität Berlin, 14195 Berlin, Germany*

‡*Institut für Weiche Materie und Funktionale Materialien, Helmholtz-Zentrum Berlin, 14109 Berlin, Germany*

¶*Biomaterials Department, Max Planck Institute of Colloids and Interfaces, 14476 Potsdam, Germany*

E-mail: rnetz@physik.fu-berlin.de

1 Equilibration and sampling

Sampling of the phase space is a major issue in all MD simulations of hydrated membranes, especially when it comes to low hydration levels. In Fig. S1 we demonstrate that our system is equilibrated, since there is no drift in any of the structural quantities, represented by the mean tilt angle $\langle\theta\rangle$ of the P-N-vector in the headgroup, the simulation box area A and the lamellar repeat distance D. Also the system enthalpy H is constant, which means that there are no major rearrangements of the bilayer structure occurring. On the other hand, we see fluctuations around the mean in these structural quantities on time scales of more than 100 ns. This is quantified in Fig. S2, where the autocorrelation functions

$$C(t) = \frac{1}{C_0\,(T-t)} \int_0^{T-t} \mathrm{d}t' X(t'+t)X(t') \qquad \text{with} \qquad C_0 = \frac{1}{T}\int_0^T \mathrm{d}t' X^2(t') \tag{S1}$$

are shown. Here, T denotes the simulation length and X the quantity of interest. All autocorrelations decay on time scales of approximately $100 - 200$ ns, hence a trajectory that sufficiently samples all configurations would require to be of a length of several hundred nanoseconds. For this reason we base our analysis on 20 independently constructed structures that are each simulated for 5 ns to assure that we are sampling the entire configuration space in a reasonable computation time.

2 Exponential fits to published experimental pressure data

In Table S1 the parameters for fits of $p = p_0 \exp\left(-D_\mathrm{w}/\lambda\right)$ to the published experimental pressure data in Fig. 1 are presented.

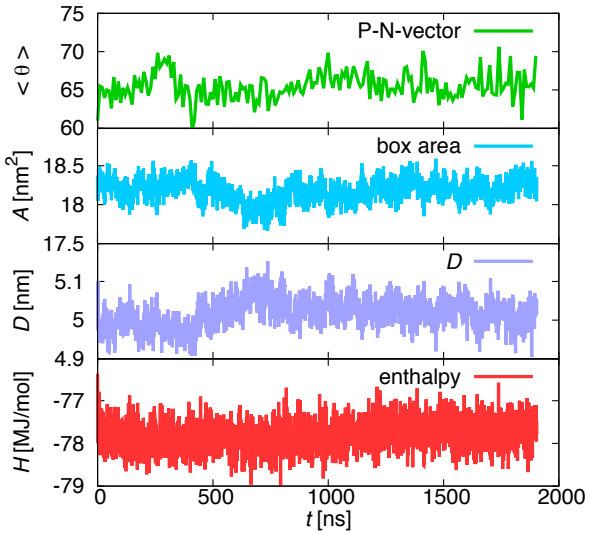

Figure S1: From top to bottom: The average tilt angle $\langle\theta\rangle$ of the P-N–vector, the simulation box area A, the lamellar repeat distance D and the system enthalpy H as a function of time for a 1.9 μs long simulation of a lipid bilayer in the gel phase with 4 water molecules per lipid.

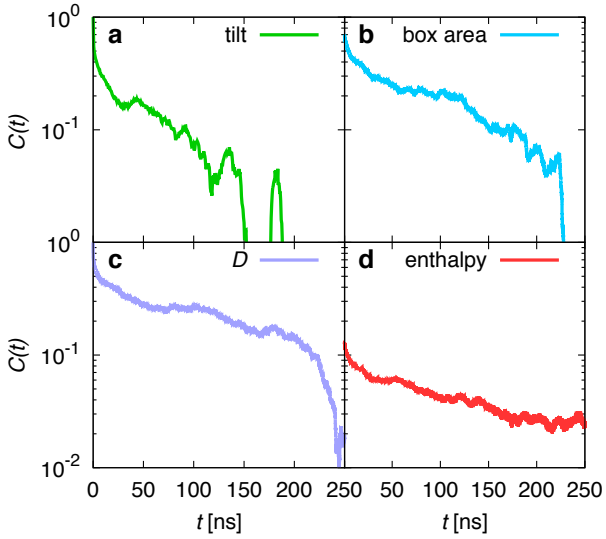

Figure S2: Normalized autocorrelation functions defined in Eqn. S1 of the average tilt angle $\langle\theta\rangle$ of the P-N–vector (**a**), the simulation box area A (**b**), the lamellar repeat distance D (**c**) and the system enthalpy H (**d**) as a function of time for a 1.9 μs long simulation of a lipid bilayer in the gel phase with 4 water molecules per lipid.

Table S1: Parameters for fits of $p = p_0 \exp(-D_\mathrm{w}/\lambda)$ to the published experimental data in Fig. 1 (a) (main text).

group	λ [nm]	$\Delta\lambda$ [nm]	$\ln p_0$ [ln bar]	$\Delta \ln p_0$ [ln bar]
Lis 25 °C	0.176	0.011	9.47	0.57
McIntosh 20 °C	0.108	0.004	10.18	0.27
Lis 50 °C	0.258	0.010	10.06	0.39
Gawrisch 50 °C	0.224	0.013	10.61	0.50
Petrache 50 °C	0.175	0.012	7.12	0.43

3 Conversion of D to D_w

3.1 Method by Lis et al.

Lis et al.[S1] use lipid–water mixtures of known lipid weight fraction Φ_L and measure the lamellar repeat distance D by X-ray diffraction. The water slab thickness is then given by

$$D_\mathrm{w}^\mathrm{Lis} = \frac{D}{1 + \frac{\Phi_\mathrm{L} v_\mathrm{L}}{(1-\Phi_\mathrm{L}) v_\mathrm{w}}}\,, \tag{S2}$$

where v_w and v_L denote the partial specific volumes of water and lipids, respectively. For water, a value of $v_\mathrm{w} = 1\,\mathrm{cm}^3/\mathrm{g}$ is used independent of D_w, whereas for the lipids in the gel and the fluid phase the values from the work of Tardieu et al. are taken[S2]. There it is assumed that a hydrocarbon chain in the gel state takes 0.95 the volume of a chain in the fluid state. Since the inverse density of a membrane in the fluid state is $v_\mathrm{L}^\mathrm{fluid} = 1\,\mathrm{cm}^3/\mathrm{g}$, we hence arrive at a value of $v_\mathrm{L}^\mathrm{gel} = 0.95\,\mathrm{cm}^3/\mathrm{g}$ for the gel phase. Furthermore, it is assumed that the membrane is incompressible in both phases, thus these values do not change with hydration. From our simulations we obtain values of $v_\mathrm{L}^\mathrm{gel} = 0.94 - 0.95\,\mathrm{cm}^3/\mathrm{g}$ and $v_\mathrm{L}^\mathrm{fluid} = 1.03 - 1.04\,\mathrm{cm}^3/\mathrm{g}$, which are not too different from these assumptions (see Fig. S3).

Lis et al.[S1] report the molecular force between two lipids instead of the pressure. From the area per lipid as a function of the lipid weight concentration, which is also measured in their work, we transform the reported force into a pressure.

As already mentioned in the main text, we choose the method introduced by Lis et

al. to transform all experimental data from D to D_w, since it allows for an unambiguous determination of the water content between the membranes. In all other works the exact water content between the membranes is not determined.

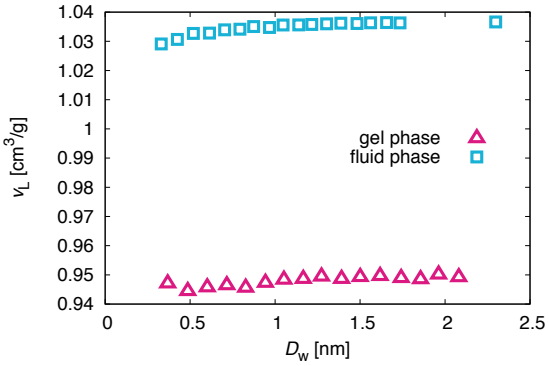

Figure S3: Partial specific volume v_L of DPPC as obtained from the simulations in the gel state (triangles) and the fluid state (squares) under the assumption that v_w is independent of D_w.

3.2 Method by McIntosh and Simon

McIntosh et al.[S3] determine the water slab thickness from X-ray diffraction experiments. In their work, they fit continuous structure amplitude functions to the measured data. These functions are then Fourier transformed to obtain electron density profiles for egg phosphatidylcholine bilayers that are used to calculate the bilayer thickness D_l as well as the bilayer repeat distance D. Specifically, using space-filling models, it is assumed that the distance between the electron density peaks plus 1 nm equals the membrane thickness D_l. The water slab thickness then follows as $D_\mathrm{w}^\mathrm{McInt.} = D - D_\mathrm{l}$. Our simulations (Fig. S4) are consistent with a constant membrane peak distance for the lipid density profiles in the gel phase, in agreement with experiments[S4]. Only pressures larger than 1000 bar lead to a slight increase of the peak distance in z-direction, which is also in agreement with experimental findings[S3].

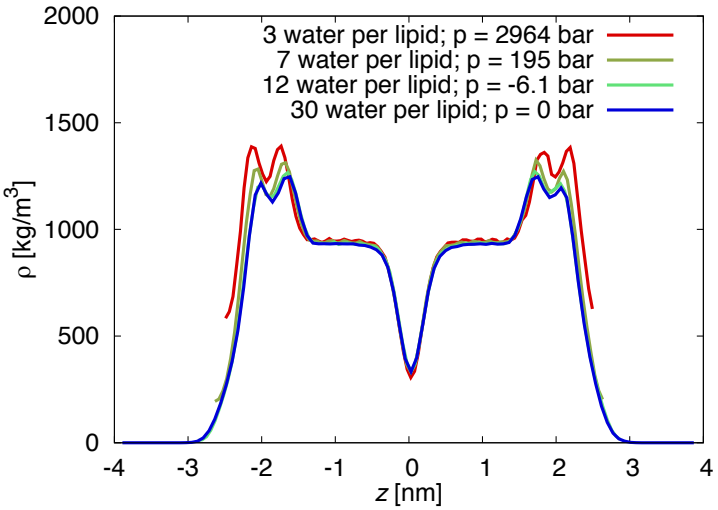

Figure S4: Density profiles of DPPC lipids obtained from simulations at four hydration levels in the gel phase.

3.3 Methods by Petrache et al. and Gawrisch et al.

Petrache et al.[S5] as well as Gawrisch et al.[S6] use the bilayer area compressibility K to calculate the bilayer thicknesses[S7]. They derive the relation

$$D_\mathrm{l}/D_\mathrm{l}^\star = \frac{K + (p - p^\star)D}{K + (p - p^\star)D_\mathrm{l}^\star} \tag{S3}$$

with which they obtain the bilayer thickness D_l without measuring the lipid weight fraction Φ_L of the lipids. In order to apply this formula, they use the bilayer thickness $D_\mathrm{l}^\star$ for one reference pressure $p^\star$. The reference values $D_\mathrm{l}^\star$ and $p^\star$ are obtained either by a measurement at one reference weight fraction (Gawrisch et al.[S6]) or by X-ray diffraction (Petrache et al.[S5]).

3.4 Back conversion

As shown above, each experimental group uses a different method to convert D to D_w, which relies on structural quantities or additional assumptions. However, a transformation from $p(D)$ data to $p(D_\mathrm{w})$ data using one conversion method for all data sets is not straightforward, since the needed experimental specifications are not published in all papers. Hence, for

example, the conversion method of Lis et al.[S1] cannot be applied directly to the published $p(D)$ data by McIntosh and Simon[S3], since the weight fractions are not published. We thus use a quadratic function of the form $D(D_\mathrm{w}) = aD_\mathrm{w}^2 + bD_\mathrm{w} + c$ to fit the relation between D and D_w for each experimental data set, which allows to interconvert all experimental data between different definitions of D_w. The resulting graphs are presented in Fig. S5 and the fitting parameters are listed in Table S2.

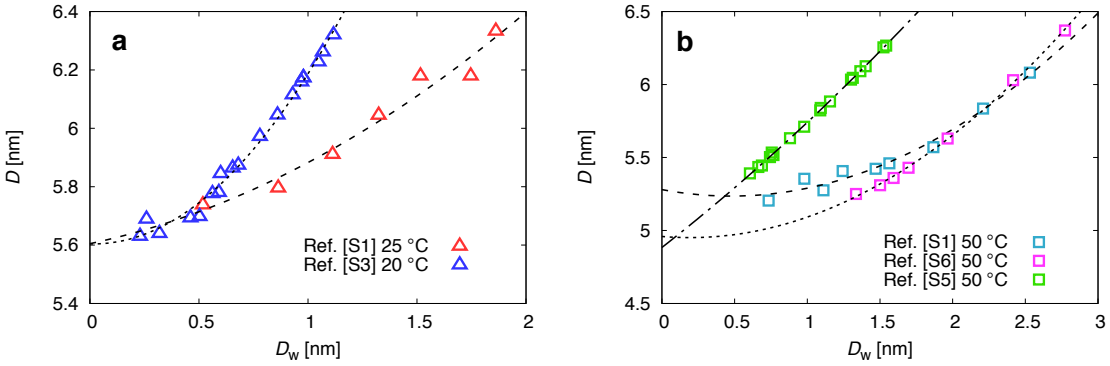

Figure S5: Lamellar repeat distance D as a function of the water slab thickness D_w for the gel phase (**a**) and the fluid phase (**b**) obtained from different experiments. To all data sets we fit a function of the form $D(D_\mathrm{w}) = aD_\mathrm{w}^2 + bD_\mathrm{w} + c$. Note that for the data representation in Fig. 3 in the main text, only the fits to the data of Lis et al. are needed.

Table S2: Parameters of fits according to $D(D_\mathrm{w}) = aD_\mathrm{w}^2 + bD_\mathrm{w} + c$ of experimental data in Fig. S5.

group	a [1/nm]	b	c [nm]
Lis 25 °C	0.119	0.159	5.60
McIntosh 20 °C	0.603	−0.020	5.60
Lis 50 °C	0.197	−0.187	5.28
Gawrisch 50 °C	0.214	−0.081	4.96
Petrache 50 °C	0.078	0.780	4.88

4 Data conversion using the method of Lis et al.

Table S3 shows the results of the fits of the function $p = p_0 \exp(-D_\mathrm{w}/\lambda)$ to the pressure distance curves after application of the conversion method used by Lis et al[S1].

Table S3: Parameters of fits according to $p = p_0 \exp(-D_\mathrm{w}/\lambda)$ of the experimental and simulation data in Fig. 3 in the main text.

	Experiments gel	Simulation 300 K	Experiments fluid	Simulation 330 K
ln p_0 [ln bar]	8.72	9.51	7.00	7.69
$\Delta \ln p_0$ [ln bar]	0.20	0.31	0.37	0.18
λ [nm]	0.207	0.222	0.384	0.363
$\Delta\lambda$ [nm]	0.007	0.021	0.026	0.028

5 Thermodynamic extrapolation

The Gibbs–Duhem equation for bulk water, $N_\mathrm{w}\mathrm{d}\mu = -S\mathrm{d}T + V\mathrm{d}p$, evaluated at constant temperature yields

$$\left(\frac{\partial\mu}{\partial p}\right)_T = \frac{V}{N_\mathrm{w}} = v_\mathrm{w}(p)$$
$$\Rightarrow \quad \Delta\mu = \mu_\infty - \mu = \int_p^{p\infty} v_\mathrm{w}(p')\,\mathrm{d}p'\,, \tag{S4}$$

with the molar volume of water v_w and the interaction pressure p that acts between the membranes. For pressures up to kilobars the water compressibility can be practically neglected[S8], hence Eq. S4 simplifies to

$$\Delta\mu = v_\mathrm{w}\,(p_\infty - p) = -v_\mathrm{w}^0 p\,, \tag{S5}$$

where the pressure p_∞ in the bulk reference system can be neglected and is set to zero. Thus in bulk water a reduced chemical potential is equivalent to a reduced pressure. We use the same equation to convert measured chemical potentials in the osmotic ensemble at $p = 1\,\mathrm{bar}$ to equivalent osmotic pressures, exactly as is done in experiments that use osmotic pressure techniques.

6 Technical details on interaction decomposition

The decomposition of the hydration repulsion is done by rerunning simulation trajectories where the simulation box is expanded in the z-direction such that on each side of the water slab, which is in the center of the box, there is only one monolayer of the membrane. This way interactions with periodic images are eliminated. In order to measure the direct contribution p_{dir}, also the water slab is removed, thus only the opposing membrane monolayers that interact with each other across free space are left, see Fig. S6 (b). The force acting on one of the monolayers divided by the area gives the direct contribution to the hydration pressure. In order to obtain the indirect contribution p_{ind}, one monolayer is removed instead of the water, and again the force acting on the remaining monolayer is measured (Fig. S6 (c)). As a consistency check of our decomposition scheme, we compare the total pressure p from the simulations with the sum of the pressure contributions $p_{\mathrm{dir}} + p_{\mathrm{ind}}$ and find perfect agreement.

Because a decomposition of the chemical potential into direct and indirect contributions is not possible, the composition into direct and indirect pressure contributions is done in the hydrostatic ensemble, where the pressure of the system is chosen such that the water chemical potential is constant.

7 Force field dependence of the simulation results

In order to investigate the dependence of our results on the employed force field, we also performed simulations with the CHARMM36UA[S9] lipid force field and using the TIP3P water model[S10], which carries additional Lennard-Jones sites on the H-atoms. In order to determine the chemical potential of this water model, also for the van-der-Waals interactions the TI method is used. For the CHARMM36UA force field, the input parameters from the NMRLipid project[S11,S12] are converted with the PyTopol script in order to make this force field compatible with Gromacs. In Fig. S7 (a) we compare the data from Fig. 3 (b) in the main text, including experimental data for fluid membranes and our simulation results

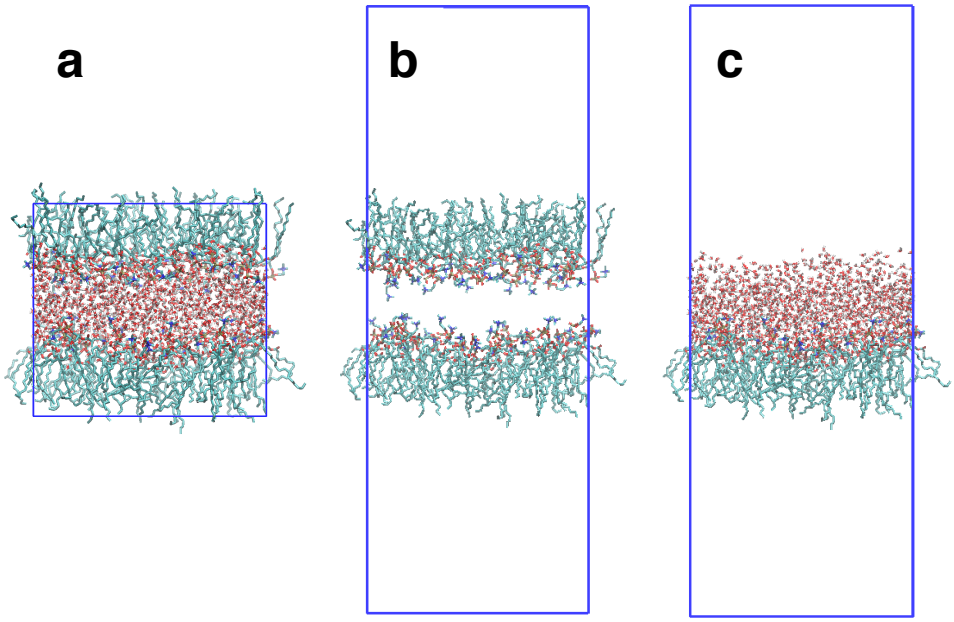

Figure S6: Decomposition of the original system (**a**) into a system without water (**b**), in which the direct contribution p_{dir} is measured, and a system with only one monolayer (**c**), in which the indirect contribution p_{ind} to the hydration pressure is measured. The blue boxes indicate the size of the simulation box.

obtained with the Berger force field, with simulation results using the CHARMM36UA force field. Both simulation results are in very good agreement with each other and also with the experimental data.

In Fig. S7 (b) we compare simulation data for the direct and indirect pressures using the CHARMM36UA force field with the pressures from Fig. 4. Here we observe that both pressure contributions $-p_{\mathrm{dir}}$ and p_{ind} have a slightly larger decay length in the CHARMM36UA force field compared to the Berger force field. But qualitatively the picture does not change: Both pressure contributions nearly cancel each other and have a much larger amplitude than the total pressure p in Fig. S7 (a). We hence conclude that our results are robust with respect to changes in the force field.

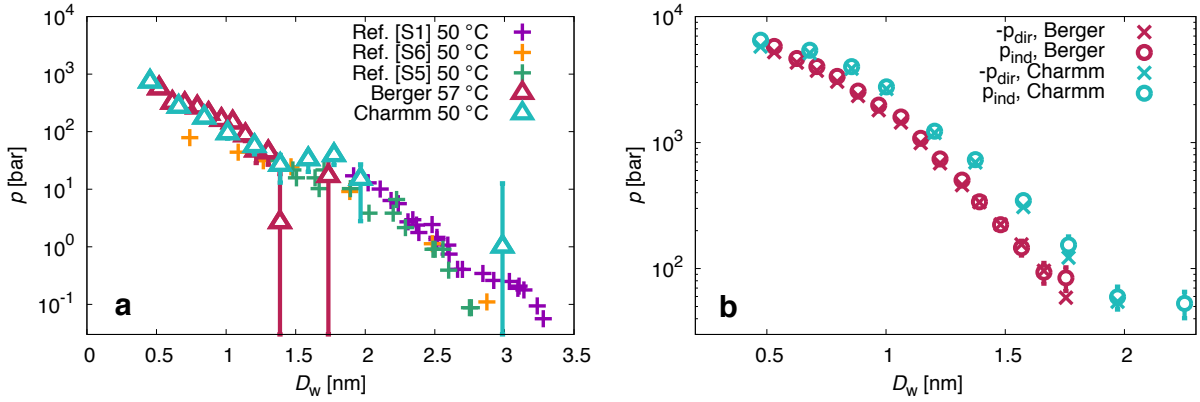

Figure S7: Comparison of the Berger force field and the CHARMM36UA force field: (**a**), Hydration pressures obtained from both force fields in the fluid phase compared to the experimental results taken from Fig. 3 (b) in the main text. (**b**), Decomposition of the pressures from both force fields into direct and indirect contributions $-p_{\mathrm{dir}}$ and p_{ind}.

References

(S1) Lis, L.; McAlister, M.; Fuller, N.; Rand, R.; Parsegian, V. Interactions between neutral phospholipid bilayer membranes. *Biophys. J.* **1982**, *37*, 657.

(S2) Tardieu, A.; Luzzati, V.; Reman, F. Structure and polymorphism of the hydrocarbon chains of lipids: A study of lecithin-water phases. *J. Mol. Biol.* **1973**, *75*, 711 – 733.

(S3) McIntosh, T. J.; Simon, S. A. Contributions of hydration and steric (entropic) pressures to the interactions between phosphatidylcholine bilayers: Experiments with the subgel phase. *Biochemistry* **1993**, *32*, 8374–8384.

(S4) McIntosh, T. J.; Magid, A. D.; Simon, S. A. Steric repulsion between phosphatidylcholine bilayers. *Biochemistry* **1987**, *26*, 7325–7332.

(S5) Petrache, H. I.; Gouliaev, N.; Tristram-Nagle, S.; Zhang, R.; Suter, R. M.; Nagle, J. F. Interbilayer interactions from high-resolution x-ray scattering. *Phys. Rev. E* **1998**, *57*, 7014–7024.

(S6) Gawrisch, K.; Ruston, D.; Zimmerberg, J.; Parsegian, V.; Rand, R.; Fuller, N. Mem-

brane dipole potentials, hydration forces, and the ordering of water at membrane surfaces. *Biophys. J.* **1992**, *61*, 1213 – 1223.

(S7) Rand, R.; Parsegian, V. Hydration forces between phospholipid bilayers. *Biochim. Biophys. Acta - Biomembranes* **1989**, *988*, 351 – 376.

(S8) Schneck, E.; Sedlmeier, F.; Netz, R. R. Hydration repulsion between biomembranes results from an interplay of dehydration and depolarization. *Proc. Natl. Acad. Sci.* **2012**, *109*, 14405–14409.

(S9) Lee, S.; Tran, A.; Allsopp, M.; Lim, J. B.; Hénin, J.; Klauda, J. B. CHARMM36 united atom chain model for lipids and surfactants. *J. Phys. Chem. B* **2014**, *118*, 547–556.

(S10) Jorgensen, W. L.; Chandrasekhar, J.; Madura, J. D.; Impey, R. W.; Klein, M. L. Comparison of simple potential functions for simulating liquid water. *J. Chem. Phys.* **1983**, *79*, 926–935.

(S11) Loison, C. Hydrated DPPC, MD simulation trajectory and related files for UA charmm36 model by Lee et al 2014. 2015.

(S12) Botan, A.; Favela-Rosales, F.; Fuchs, P. F. J.; Javanainen, M.; Kanduč, M.; Kulig, W.; Lamberg, A.; Loison, C.; Lyubartsev, A.; Miettinen, M. S.; Monticelli, L.; Määttä, J.; Ollila, O. H. S.; Retegan, M.; Róg, T.; Santuz, H.; Tynkkynen, J. Toward Atomistic Resolution Structure of Phosphatidylcholine Headgroup and Glycerol Backbone at Different Ambient Conditions. *J. Phys. Chem. B* **2015**, *119*, 15075–15088.